PHYSICAL REVIEW B VOLUME 4, NUMBER 8 15 OCTOBER 1971

Interband Electronic Raman Scattering in Semimetals and Semiconductors

E. Burstein*
Department of Physics and Laboratory for Research on the Structure of Matter, University of Pennsylvania, Philadelphia, Pennsylvania 19104

and

D. L. Mills* and R. F. Wallis
Department of Physics, University of California, Irvine, California 92664
(Received 2 April 1971)

In this paper we examine the inelastic scattering of light by interband electronic transitions (interband electronic Raman scattering) in semiconductors and semimetals. A number of general features of the scattering process and the resulting Raman spectrum are examined. We also present detailed calculations of the form and magnitude of the Raman efficiency associated with interband transitions near the Γ point of the Brillouin zone in materials with the gray-tin band structure in zero magnetic field.

I. INTRODUCTION

The study of inelastic scattering of light by electrons in solids (electronic Raman scattering) has provided a powerful means of studying electronic properties. Since electronic Raman scattering is a second-order process, there are three types of electronic states involved—namely, initial, intermediate, and final states. If the initial and final states of the electron are in the same energy band, the scattering is an *intraband* electronic Raman scattering. A number of examples of intraband electronic Raman scattering have been studied, particularly in semiconductors. These include single-particle[1] scattering by conduction electrons or holes, spin-flip[2] scattering, inter-Landau-level[3] scattering, and impurity[4] scattering.

Another possibility, which has received relatively little attention, is interband electronic Raman scattering,[5] in which the initial and final electronic states are in different bands. In the general situation, the initial, intermediate, and final states are each in different energy bands. This is illustrated in Fig. 1. Under special circumstances, however, the intermediate states may be in the same band as either the initial or the final state. In this case, one of the transitions is an intraband transition, and a perturbation such as an external magnetic field, an impurity potential, or the Coulomb interaction of the electron and hole (exciton[6] effects) is required.

Considerations of crystal symmetry impose selection rules on interband Raman scattering. For crystals with a center-of-inversion symmetry and in the absence of perturbations such as an external magnetic field, strong interband scattering associated with transitions at high symmetry points will occur, in the limit of zero wave vector of the photons, only if the initial and final states are in bands of the *same* parity. Consequently, familiar semiconductors such as Ge do not exhibit strong scattering associated with direct transitions between the valence band and the conduction band at $\vec{k}=0$. In a III-V compound such as InSb, which lacks a center-of-inversion symmetry, interband scattering is in principle allowed, but may be relatively weak because lack-of-center-of-inversion effects in InSb are generally small. On the other hand, cuprous oxide is an example

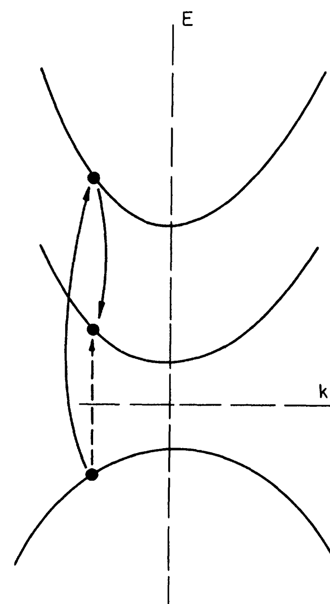

FIG. 1. Illustration of the two electronic transitions involved in the three-band case of interband electronic Raman scattering. Each transition conserves momentum of the electron and photon. Dashed arrow indicates the net electronic excitation.

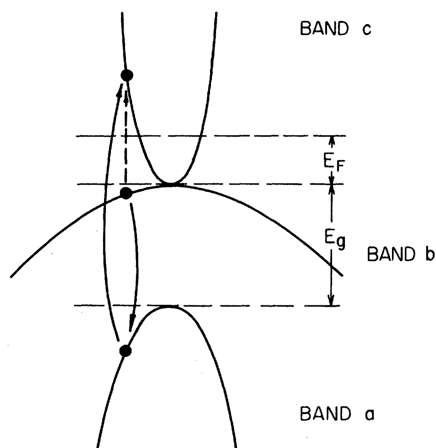

FIG. 2. Band structure of gray tin near the Γ point of the Brillouin zone. The two transitions that give rise to interband electronic Raman scattering considered in this paper are indicated. Dashed arrow indicates the net electronic excitation.

of a material which has valence and conduction bands of the same parity and which should show strong interband Raman scattering. A special case of interest where three different bands are involved is that of germanium or indium antimonide, where the initial and final states are in two of the upper valence bands derived from p-like atomic states. For this situation, free holes are required. It should be noted that the parity selection rules for interband Raman scattering are complementary to those for interband optical absorption in that the scattering involves transitions between bands of the same parity whereas the absorption involves transitions between bands of opposite parity.

Interband Raman scattering between valence and conduction bands is possible in Ge and InSb for $\vec{k} \neq 0$. The matrix element is proportional to the wave vector $\vec{k}$ for small values of $\vec{k}$, and the scattering should be smaller than when two direct allowed transitions are involved. For large values of $\vec{k}$, however, the scattering can be quite appreciable. Application of an external magnetic field is another way of breaking down parity selection rules.[7] Furthermore, the magnetic field introduces singular structure into the spectrum of scattered radiation which can be useful in identifying interband Raman scattering. For noncentrosymmetric crystals of sufficiently low symmetry, such as CdS, no parity selection rules exist and strong interband scattering should be possible at all points in the Brillouin zone.

A calculation of interband Raman scattering in an external magnetic field has recently been carried out by two of the present authors.[7] In this case one has an interband transition and an intraband transition between Landau levels in contrast to the case considered in Sec. II where two interband transitions are involved. The Raman cross section for the magnetic field case exhibits a strong resonance when the frequency of the scattered light equals the cyclotron frequency. However, since one of the transitions involves an intraband transition between Landau levels, the intensity of the scattering is smaller than for materials where both transitions can be interband at $\vec{k} = 0$.

In this paper we focus our attention on transitions near the band edges of semiconductors whose direct band edges have the same parity. The phenomena are relatively simple and uncomplicated by competing processes which occur at larger energies. Some materials particularly suited for this purpose are gray tin and mercury telluride which have zero energy gaps. The uppermost valence band and the lowest conduction band have the same parity, so strong scattering is expected.

A sketch of the valence- and conduction-band extrema for gray tin is shown in Fig. 2. Groves and Paul[8] have argued that a structure of this nature near the Γ point of the Brillouin zone is required by the available transport and optical data for this system. We denote the three bands as band (a), band (b) and band (c), as indicated in Fig. 2. This band structure is obtained from the germanium band structure by allowing the energy gap between the Γ_2 and Γ_{25} bands to assume a negative value. The light mass band (a) of Fig. 2 has wave functions at Γ identical to those of the germanium conduction band. Band (b) and band (c) have wave functions at Γ identical to the heavy and light hole bands in germanium, respectively. In the absence of carriers at zero temperature, the Fermi energy E_F in Fig. 2 assumes the value zero; band (b) is therefore filled and band (c) is empty at $T = 0\,°K$. Gray tin is thus a semiconductor with a direct gap that is zero in magnitude.

Direct optical transitions of the type (a)→(b) and (a)→(c) are allowed by symmetry, and therefore the Raman process indicated in Fig. 2 can occur. In the first step, the incident photon of frequency ω_0 induces a direct transition between the filled band (a) and an empty state in the conduction band (c). In the second step, a electron from state (b) drops into the hole created by the first transition and emits the scattered photon of frequency ω_1. The frequency shift $\omega = \omega_0 - \omega_1$ is equal to the excitation energy of the particle-hole pair created in the scattering process. Alternatively, the roles of the incident and scattered photons can be interchanged. In Sec. II, we present a theoretical calculation of the interband Raman scattering in gray tin.

II. DERIVATION OF RAMAN EFFICIENCY

In this section, we derive an expression for the

scattering intensity associated with the process illustrated in Fig. 2. Since the calculation is a straightforward one, and we employ standard theoretical techniques used elsewhere,[7,9] we shall omit the details, and sketch only the key features of the manipulations.

Upon treating the $\vec{p}\cdot\vec{A}$ term in the Hamiltonian in the second Born approximation, one may derive an expression for the differential scattering cross section per unit solid angle per unit frequency by following Yafet's method.[9] From this expression, we form the quantity $d^2S/d\Omega\, d\omega$, the Raman efficiency per unit solid angle per unit frequency per unit length. If an incident photon travels a distance of 1 cm in the crystal, then the probability that it is scattered via the Raman process into the solid angle $\Delta\Omega$, with frequency shift between ω and $\omega + \Delta\omega$ is given by $(d^2S/d\Omega\, d\omega)\Delta\Omega\,\Delta\omega$. We find that

$$\frac{d^2S}{d\Omega\, d\omega} = \left(\frac{e^2}{mc^2}\right)^2 \left(\frac{m_b m_c}{m_b + m_c}\right)^{3/2} \frac{\omega^{1/2}(\omega_0 - \omega)}{4(2^{1/2})\pi^3\omega_0\hbar^{3/2}} \times \sum_{\sigma_1\sigma_2}\int d\Omega(\hat{k}) \left| \frac{1}{mA}\sum_{\sigma''}\langle c\sigma_2\hat{k}|p_I|a\sigma''\rangle\langle a\sigma''|p_S|b\sigma_1\hat{k}\rangle + \frac{1}{mB}\sum_{\sigma''}\langle c\sigma_2\hat{k}|p_S|a\sigma''\rangle\langle a\sigma''|p_I|b\sigma_1\hat{k}\rangle\right|^2 . \tag{1}$$

In Eq. (1), m_b and m_c are the magnitudes of the effective masses associated with band (b) and band (c), respectively, and m is the free-electron mass. The frequency shift of the scattered light is ω, the frequency of the incident light is ω_0, and we have defined the quantities

$$A = E_g + \hbar\omega\left(\frac{m_b(m_a + m_c)}{m_a(m_b + m_c)}\right) - \hbar\omega_0 ,$$

$$B = E_g + \hbar\omega\left(\frac{m_c(m_b - m_a)}{m_a(m_b + m_c)}\right) + \hbar\omega_0 .$$

The quantities p_I and p_S are projections of the momentum operator $\vec{p}$ on the direction of polarization of the incident and scattered photon.

We compute the matrix elements that appear in Eq. (1) by employing wave functions appropriate to the point $\vec{k} = 0$ of the Brillouin zone. These wave functions may be obtained from the work of Kane[10] on the band structure of InSb near $\vec{k} = 0$ upon noting the relationship between the bands of the gray-tin structure and InSb. In this paper, of course, we omit contributions to the wave functions arising from lack of inversion symmetry. In Eq. (1), the wave function of an electron in band (a) with spin σ at the Γ point of the zone is denoted by $|a\sigma\rangle$. The wave functions of band (b) and band (c) are each mixtures of up and down spin character because of the presence of spin-orbit coupling. The indices σ_1 and σ_2 in Eq. (1) then serve as state labels, but are not to be interpreted literally as spin indices. Furthermore, since band (b) and band (c) are degenerate at $\vec{k} = 0$, the particular linear combinations of p-like functions that occur in the wave functions of these bands near $\vec{k} = 0$ depend upon the direction from which the center of the zone is approached when one takes the limit $\vec{k} \to 0$. We include this feature of the wave functions in the notation by explicitly indicating the dependence of the state vectors $|b\sigma, \hat{k}\rangle$ and $|c\sigma, \hat{k}\rangle$ on the direction of the wave vector $\vec{k}$.

Finally, in Eq. (1), the integration exhibited explicitly is over the directions of the wave vector $\vec{k}$.

In the paper by Kane,[10] the wave functions that are exhibited are those appropriate to the case where $\vec{k} \to 0$ along the z axis. It is straightforward to derive the wave functions associated with approach to the origin from a general direction in $\vec{k}$ space by applying the appropriate rotation operator to Kane's wave functions.

The process in Fig. 2 gives scattered radiation polarized both parallel to, and perpendicular to, the plane of polarization of the incident radiation. We shall consider each scattering geometry separately. Furthermore, one has $m_c \cong m_a = m^* \ll m_b$ for the band structure of Fig. 2, so we confine our attention to this limit.

A. Intensity of the *X-X* Scattering

We first consider the case where both the incident and the scattered radiation are polarized parallel to the x axis. In the limit $m_c \cong m_a = m^* \ll m_b$, Eq. (1) becomes

$$\frac{d^2S_{xx}}{d\Omega d\omega} = \left(\frac{e^2}{mc^2}\right)^2 \frac{m^{*3/2}\omega^{1/2}(\omega_0 - \omega)}{4(2^{1/2})\pi^3\omega_0\hbar^{3/2}} \left(\frac{1}{A} + \frac{1}{B}\right)^2 \times \int d\Omega(\hat{k}) \sum_{\sigma_1\sigma_2} \left| \frac{1}{m}\sum_{\sigma''}\langle c\sigma_2, \hat{k}|p_x|a\sigma''\rangle\langle a\sigma''|p_x|b\sigma_1, \hat{k}\rangle\right|^2 , \tag{2}$$

where

$$A = Eg + 2\hbar\omega - \hbar\omega_0, \qquad B = Eg + \hbar\omega + \hbar\omega_0 .$$

In terms of the quantity P introduced by Kane,[10] we find

$$\sum_{\sigma_1\sigma_2} \int d\Omega(\hat{k}) \left| \frac{1}{m^2} \sum_{\sigma''} \langle c\sigma_2, \hat{k} | p_x | a\sigma'' \rangle \langle a\sigma'' | p_x | b\sigma_1, \hat{k} \rangle \right|^2 = \frac{32\pi P^4}{45\hbar^4} .$$

Upon noting that P^2 is related to m^* via the relation

$$P^2 = \tfrac{3}{4}(Eg/m^*)\hbar^2 ,$$

when m^* is small compared to the free-electron mass m, the Raman efficiency assumes the form

$$\frac{d^2S}{d\Omega d\omega} = \left(\frac{e^2}{m^*c^2}\right)^2 \frac{m^{*3/2}\omega^{1/2}(\omega_0-\omega)}{10(2^{1/2})\pi^2\hbar^{3/2}\omega_0} \left| \frac{E_g}{E_g+2\hbar\omega-\hbar\omega_0} + \frac{E_g}{E_g+\hbar\omega+\hbar\omega_0} \right|^2 . \tag{3}$$

We shall discuss the principal features of this expression in Sec. III.

B. Intensity of X-Y Scattering

We next display the Raman efficiency for the case where the incident light is polarized parallel to the x axis, and the scattered radiation is polarized parallel to the y axis.

When $\sigma_1 = \sigma_2 = \sigma$, we find

$$\int d\Omega(\hat{k}) \left| \frac{1}{m^2 A} \sum_{\sigma''} \langle c\sigma, \hat{k} | p_x | a\sigma'' \rangle \langle a\sigma'' | p_y | b\sigma, \hat{k} \rangle + \frac{1}{m^2 B} \sum_{\sigma''} \langle c\sigma, \hat{k} | p_y | a\sigma'' \rangle \langle a\sigma'' | p_x | b\sigma, \hat{k} \rangle \right|^2 = \frac{2\pi}{15} \frac{P^4}{\hbar^4} \left(\frac{1}{A} + \frac{1}{B}\right)^2 .$$

For the case where $\sigma_1 \neq \sigma_2$,

$$\int d\Omega(\hat{k}) \left| \cdots \right|^2 = \frac{16\pi P^4}{45\hbar^4} \left(\frac{1}{A^2} + \frac{1}{B^2} - \frac{1}{2}\frac{1}{AB} \right) .$$

These two results enable the form for the scattering to be written

$$\frac{d^2S_{xy}}{d\Omega d\omega} = \frac{\sqrt{2}}{16\pi^2} \left(\frac{e^2}{m^*c^2}\right)^2 \frac{m^{*3/2}\omega^{1/2}(\omega_0-\omega)}{\hbar^{3/2}\omega_0} E_g^2 \left[\frac{1}{A^2} + \frac{1}{B^2} + \frac{1}{10}\left(\frac{1}{A} + \frac{1}{B}\right)^2 \right] , \tag{4}$$

where A and B have the same values given above.

The general results obtained above for gray tin may also be expected to be valid with change only in detail for materials such as mercury telluride.

III. DISCUSSION OF THE RESULTS FOR GRAY TIN

We observe that both parallel and perpendicular scattering are allowed for the interband scattering in gray tin. They do not, however, have a simple breakdown into spin-flip and non-spin-flip scattering as is true for the intraband case in other materials as discussed by McWhorter and Hamilton.[2] Thus, transitions are possible from either of the Kramers degenerate initial states to either of the Kramers degenerate final states for both the X-X and X-Y scattering. Whether screening plays a role in the interband case analogous to that in the intraband case remains to be investigated.

Since the expression in Eq. (4) for the Raman efficiency associated with X-Y scattering is quite similar in its qualitative features to that for X-X scattering [Eq. (3)], we confine our comments to the latter geometry. First consider the shape of the spectrum of the scattered light. From Eq. (3), one sees that this spectrum consists of a broad band spread over the entire range from $\omega = 0$ to $\omega = \omega_0$. The spectrum is quite smooth provided that $\hbar\omega_0 < E_g$. The scattering intensity varies as $\omega^{1/2}$ for $\omega \ll \omega_0$ and vanishes linearly as $\omega \to \omega_0$. The $\omega^{1/2}$ dependence is a consequence of the direct allowed transition involved and is a manifestation of the combined density of states. We emphasize that $\hbar\omega$ is the electronic excitation energy.

If $\hbar\omega_0 > E_g$, a strong resonant enhancement occurs when the frequency shift ω equals $\mu_{ac}(\omega_0 - \omega_g)/\mu_{bc}$, where μ_{ac} and μ_{bc} are the reduced effective masses of bands (a), (c) and bands (b), (c), respectively, and $\omega_g = E_g/\hbar$. When $\omega_0 > \omega_g$, the Raman spectrum acquires an intense peak centered at the value indicated above for the frequency shift ω. For the simplified band model of gray tin considered in Sec. II in which $m_c \approx m_a = m^* \ll m_b$, the resonance occurs

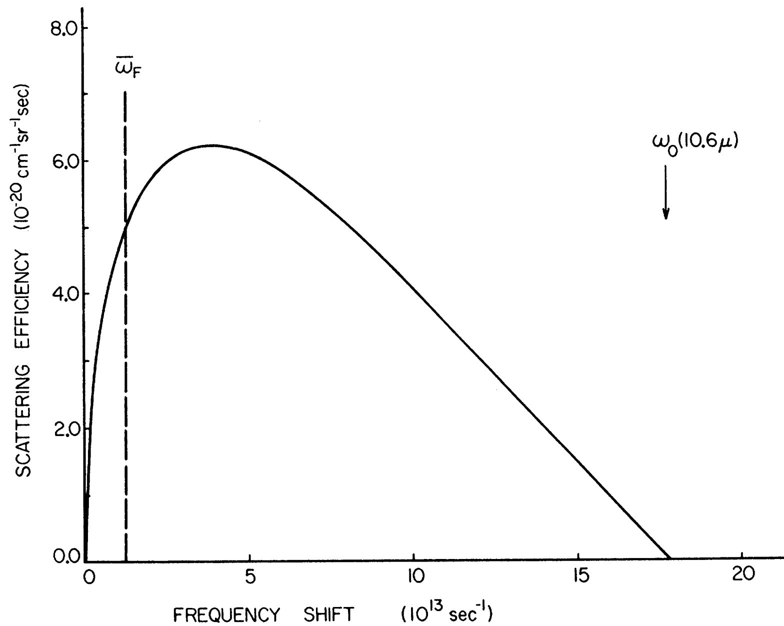

FIG. 3. Plot of the scattering efficiency per unit length per unit solid angle per unit frequency as a function of frequency shift for the case where gray tin is illuminated with radiation of wavelength 10.6 μ corresponding to $\omega_0 < \omega_g$. The cutoff that occurs at $\omega = \overline{\omega}_F$ is indicated for a conduction-electron concentration of 10^{16} cm^{-3}.

for $\omega = \frac{1}{2}(\omega_0 - \omega_g)$.

Physically, the resonance corresponds to the incident radiation producing a real transition between bands (a) and (c) for some particular wave vector and the scattered radiation producing a real transition between bands (b) and (a) for the same wave vector. From energy conservation the frequency shift ω must then be given by the above resonance condition. Knowing ω_0 and the value of ω required to produce resonance, one can then obtain an experimental value of the energy gap E_g. This resonance situation is referred to[11] as "resonance fluorescence."

In our theory the differential scattering cross section diverges at the resonance point. If one includes the finite lifetime τ of the electronic states in the calculation, a sharp peak occurs with a height proportional to τ^2 and a width proportional to τ^{-1}.

In Sec. II the discussion presumed that no carriers are present in the conduction band. If the presence of free carriers is taken into account because of impurities present in the material, their effect is to depress the spectrum below the form predicted by Eqs. (3) and (4) in the region of small frequency ω, since the final states that enter the scattering process will be blocked. The effect of a degenerate gas of electrons in the conduction band with Fermi energy $E_F > 0$ is to completely block all final states associated with scatterings for which $\omega \leq \overline{\omega}_F$, where $\overline{\omega}_F = [1 + (m_c/m_b)] E_F/\hbar$. For the simplified model of gray tin, $m_c \ll m_b$, and the onset of scattering occurs for $\omega = \omega_F = E_F/\hbar$. Thus, the shape of the spectrum is that given by Eqs. (3) and (4) for $\hbar\omega > E_F$, but the scattering intensity drops to zero abruptly when $\hbar\omega = E_F$. The presence of holes in the valence band [band (b) of Fig. 2] has precisely the same effect, since the initial states are empty near the top of the valence band. If the carrier distribution is nondegenerate, then the spectrum is depressed on the low-frequency end, without the sharp cutoff characteristic of a highly degenerate distribution.

From the foregoing discussion, we see that a resonance is possible only if the incident photon energy is greater than the energy separation E_g between the top of the s-like band and the top of the valence band. In Fig. 3 we present the spectrum of scattered radiation for the case in which the incident photon energy, corresponding to the 10.6-μ CO_2 laser line or 0.117 eV, is less than $E_g = 0.4$ eV. In this situation, $\hbar\omega_0/E_g = 0.3$. For small frequency shifts, the spectrum is dominated by the density-of-states factor $\omega^{1/2}$. At larger frequency shifts, the scattering efficiency decreases as $\omega_0 - \omega = \omega_1$ and goes to 0 when the scattered frequency ω_1 becomes 0. Also shown in Fig. 3 is the cutoff at the carrier-dependent gap due to a degenerate conduction-electron concentration of 10^{16} cm^{-3}. In the gray-tin case, the carrier-dependent gap is $\hbar\overline{\omega}_F$, but in a non-zero-gap material, it contains contributions both from the intrinsic gap and from the free carriers. Below this cutoff, the scattering efficiency is zero because of the Pauli exclusion principle. The sharp onset of scattering at $\omega = \overline{\omega}_F$ can serve as a valuable fiduciary mark to identify the interband scattering. Another point to be noted is that the second-order matrix element has little effect on the frequency dependence in Fig. 3.

A situation for gray tin which exhibits resonance

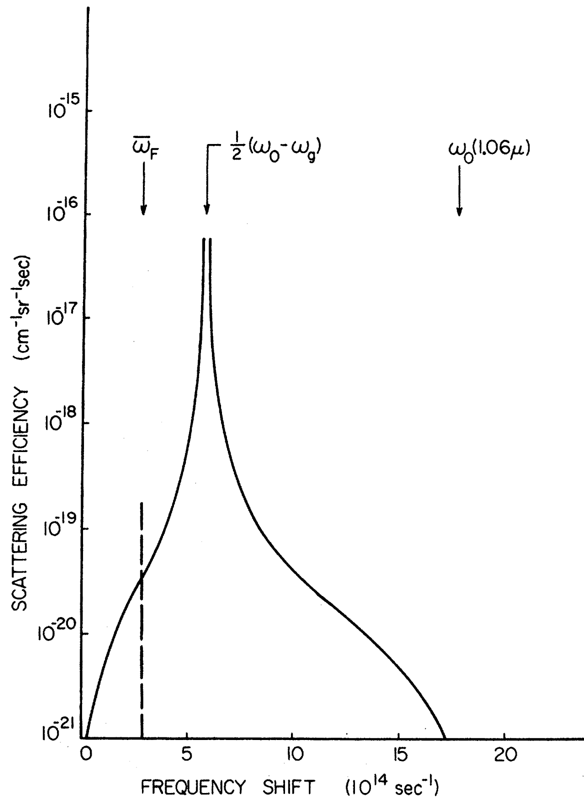

FIG. 4. Plot of the scattering efficiency per unit length per unit solid angle per unit frequency as a function of frequency shift for the case where gray tin is illuminated with radiation of wavelength 1.06 μ corresponding to $\omega_0 > \omega_g$. The cutoff that occurs at $\omega = \overline{\omega}_F$ is indicated for a conduction-electron concentration of 10^{18} cm^{-3}.

is shown in Fig. 4, where the incident frequency corresponds to the 1.06-μ line of the Nd-YAG laser and $\hbar\omega_0/E_g = 3$. From an experimental observation of the position of this peak, one can get direct information about the energy gap E_g. The cutoff at $\omega = \overline{\omega}_F$ associated with a conduction-electron concentration of 10^{18} cm^{-3} is also shown. Experimental observation of this onset of scattering provides a direct value of the reduced Fermi level.

Next consider the strength of the scattering. For the case where the incident radiation has a wavelength of 10.6 μ—i.e., the scattering is nonresonant—from Fig. 3 one estimates that the scattering efficiency per unit length per unit solid angle per unit frequency at the maximum in the Raman spectrum is

$$\frac{d^2S}{d\Omega\, d\omega} = 6\times10^{-20}\ \mathrm{cm^{-1}\,sr^{-1}\,sec}. \quad (5)$$

If one accepts all the radiation scattered into a frequency range of width $\Delta\omega = 5$ cm^{-1} with frequency shift near the maximum in the Raman spectrum, then the Raman efficiency per unit solid angle per unit length becomes

$$\frac{dS}{d\Omega} = \frac{d^2S}{d\Omega\, d\omega}\,\Delta\omega = 5\times10^{-8}\ \mathrm{cm^{-1}\,sr^{-1}}\ . \quad (6)$$

This estimate indicates that Raman scattering from interband transitions in gray tin should be of observable magnitude, even if frequencies ω_0 sufficiently small for resonance effects to be unimportant are utilized in the experiment. Quite clearly, if $\hbar\omega > E_g$, the scattering in the resonance region discussed earlier is stronger by several orders of magnitude than the estimate displayed in Eq. (6). However, when the incident frequency is that large, the optical skin depth is much smaller than that appropriate to the frequency region $\hbar\omega_0 \ll E_g$. The reduction of the scattering volume that results with the decrease in skin depth will offset some of the gain achieved by the resonant denominator, although the resonant peak should remain a sharp feature in the Raman spectrum. The dependence of skin depth on frequency will clearly modify the shape of the observed spectrum.

In the present calculation, we have treated the electron and the hole created in the scattering process within the framework of the one-electron theory of solids—i.e., exciton effects have been neglected. In many semiconductors, exciton effects will produce significant modifications in the scattering spectrum from that predicted by Eqs. (3) and (4). Well-defined peaks associated with exciton transitions should be observable. The scattering efficiency, furthermore, will not go to zero at a frequency shift corresponding to the energy gap.

We conclude this section with a remark on the possible influence of many-body corrections to the shape of the spectrum for gray tin. As indicated above, one may expect the shape of the spectrum to differ from that computed in this work if Coulomb interactions between the particle and the hole created in the scattering process are important. In particular, if the material is close to an instability with respect to an excitonic insulator phase, a severe distortion of the spectrum at small frequency transfers will occur. In the particular case of gray tin, Kohn and Sherrington[12] have estimated the exciton binding energy. Very crudely, one may expect that the region of frequency transfer over which the spectrum is severely distorted from the form predicted by the one-electron theory will be the order of the exciton binding energy. Kohn and Sherrington find that the exciton binding energy in gray tin is several orders of magnitude smaller than one would estimate on the basis of a simple hydrogenic model. The reason is that the zero band gap associated with the band structure in Fig. 2 leads to singular behavior for the wave-vector-dependent dielectric constant of

the material, in the limit as the wave vector goes to 0. This singularity has the effect of greatly reducing the strength of the effective Coulomb interaction between the excited particle and hole. Thus, the Coulomb correlations between the excited particle and hole should be very weak in gray tin, and our single-particle theory should provide an accurate description of the shape of the Raman spectrum associated with interband transitions. The presence of free carriers will diminish exciton effects further and will cut off the electronic excitations at small frequency shifts.

IV. GENERAL DISCUSSION

In this section, we discuss a number of general features of interband electronic Raman scattering, in semiconductors, with the example provided by gray tin in mind.

The scattered radiation ranges over a very wide frequency region. The upper limit to the frequency shift is determined by the frequency of the incident radiation, and the lower limit by the direct carrier-dependent band gap. This is in contrast to the case of intraband electron scattering,[1,2] where the frequency shift varies from 0 to qv_F, with q the scattering wave vector, and v_F the Fermi velocity.

Since the spectrum associated with interband electronic scattering is broad, and there are no well-defined features other than the edge at the onset of scattering and the resonance peak, it may be difficult to distinguish between interband scattering and other processes which lead to the emission of radiation in this spectral region—i.e., luminescence.

Application of magnetic field will introduce structure into the Raman spectrum. This will enable one to obtain further information about the band structure, just as one does in interband magneto-optical absorption. In the case of interband electronic Raman transitions between bands of the same parity, a magnetic field introduces structure into the spectrum (i.e., interband transitions between Landau levels) similar in character to the structure introduced in the magneto-absorption spectrum associated with direct allowed interband transitions, in which each pair of Landau levels n, n' contributes a feature which beyond the onset frequency $\omega_{nn'}$ is proportional to $(\omega - \omega_{nn'})^{-1/2}$. The study of the magnetic-field-induced structure in the Raman spectrum provides an additional means of obtaining information about the energy-band parameters. Furthermore, in a magnetic field, the resultant structure provides a means of identifying the scattering process responsible for the radiation. For both gray tin and HgTe, the relaxation times are sufficiently long to permit easy observation of the magnetic structure in the interband scattering. Such structure has already been observed in interband absorption.[13] A detailed theoretical study of interband electronic Raman scattering in a strong magnetic field has been carried out for the case in which direct transitions between the valence and conduction band are allowed, and the Raman process consists of a sequence of an interband transition, and an intraband (cyclotron resonance) transition.[7]

A case similar to the one treated in the present paper is the interband scattering that can occur between the V_1 and V_2 bands of materials like Ge or GaAs; since the initial and final electronic states are in the valence band, holes must be present for the scattering to occur. The selection rules for this process are similar to those for the gray-tin and HgTe case. The case of the scattering between the V_1 and V_2 bands in Ge and GaAs is particularly convenient, since there are regions of transparency for incident frequencies below the intrinsic absorption edge, whereas in the gray-tin or HgTe case the material is opaque. Intraband scattering by holes in GaAs has been reported by Mooradian[1] under conditions with $\hbar\omega_0 < E_g$. To distinguish the inter-valence-band scattering from the intraband scattering of holes, it would be necessary to employ a magnetic field to induce structure in the interband portion of the spectrum or use forward scattering in the limit $q = 0$, where the interband but not the intraband scattering will persist.

One of the principal problems in observing interband Raman scattering is distinguishing this scattering from ordinary luminescence. Since electron-hole pairs are produced in the Raman process, there may be recombination of the electrons and holes with the emission of light. The electrons and holes have a certain lifetime during which they may partially or completely thermalize before recombining. A broad luminescence band may therefore be expected. The distinction between the Raman scattering and luminescence may be facilitated by using the positions of the resonance peak or the peaks in the presence of a magnetic field as fiduciary marks, and following their shift with change in the incident frequency.

---

*Research supported in part by the U. S. Army Research Office, Durham, N. C.

†Research sponsored by the Air Force Office of Scientific Research, Office of Aerospace Research, USAF, under Grant No. AFOSR 70-1936.

[1]A. Mooradian, in *Light Scattering Spectra of Solids*, edited by G. B. Wright (Springer, New York, 1969), p. 285.

[2]D. C. Hamilton and A. L. McWhorter, in Ref. 1, p. 309; C. K. N. Patel and E. D. Shaw, Phys. Rev. Letters 24, 451 (1970).

[3]P. A. Wolff, Phys. Rev. Letters 16, 225 (1966); Y.

Yafet, Phys. Rev. 152, 858 (1966); R. E. Slusher, C. K. N. Patel, and P. A. Fleury, Phys. Rev. Letters 18, 77 (1967).

[4]R. J. Elliott and R. Loudon, Phys. Letters 3, 189 (1963); C. H. Henry, J. J. Hopfield, and L. C. Luther, Phys. Rev. Letters 17, 1178 (1966); G. B. Wright and A. Mooradian, *ibid.* 18, 608 (1967).

[5]S. S. Jha, Nuovo Cimento 63B, 331 (1969); E. Burstein, A. Pinczuk, and R. F. Wallis, Phys. Chem. Solids Suppl. 32, 251 (1971).

[6]R. J. Elliott and R. Loudon, Phys. Letters 3, 189 (1963).

[7]R. F. Wallis and D. L. Mills, Phys. Rev. B 2, 3312 (1970).

[8]S. Groves and W. Paul, in *Physics of Semiconductors*, edited by M. Hulin (Dunod Cie., Paris, 1964), p. 41.

[9]Y. Yafet, Phys. Rev. 152, 858 (1966).

[10]E. O. Kane, J. Phys. Chem. Solids 1, 249 (1957).

[11]W. Heitler, *Quantum Theory of Radiation*, 3rd ed. (Oxford U. P., Oxford, England, 1954), p. 196.

[12]D. Sherrington and W. Kohn, Rev. Mod. Phys. 40, 767 (1968).

[13]S. H. Groves, C. R. Pidgeon, A. W. Ewald, and R. J. Wagner, J. Phys. Chem. Solids 31, 2031 (1970).

PHYSICAL REVIEW B VOLUME 4, NUMBER 8 15 OCTOBER 1971

Quantum Transport Theory of Impurity-Scattering-Limited Mobility in *n*-Type Semiconductors Including Electron-Electron Scattering*

Mark Luong and Alan W. Shaw
Electrical Engineering Department, Utah State University, Logan, Utah 84321

(Received 6 May 1971)

The Kubo formula is employed to obtain an expression for ionized-impurity mobility, including higher-order impurity scattering effects and electron-electron scattering effects for nondegenerate semiconductors. Without electron-electron scattering, the lowest-order term of the mobility, as has been previously demonstrated, is found to be the same as the well-known Brooks-Herring formula for ionized-impurity mobility. The form of the higher-order impurity scattering terms has also been previously given. We have evaluated these terms and found them to be negligibly small for the range of impurity concentration and temperature considered here. Electron-electron scattering is calculated by a single-particle approximation from the time-independent Hartree-Fock theory, taking the electron-impurity scattering as the basic mechanism and treating the electron-electron interactions as perturbations. An impurity-scattered electron in our model is found to interact only with other independent electrons not interacting with impurities. Taking into account the correction of electron-electron scattering effects, the Brooks-Herring formula is found to be reduced by a factor which can be expressed in closed form as $1-e^{-1}$. This factor of 0.632 agrees well with other theoretical calculations using the Boltzmann transport theory.

I. INTRODUCTION

Two theoretical treatments have been proposed to describe ionized-impurity-scattering-limited mobility in semiconductors: the Conwell-Weisskopf[1] and Brooks-Herring[2-6] treatments. These two different approaches yield nearly the same result. While these formulas are qualitatively correct, there are refinements by which they may be improved. One of these improvements involves taking into account the electron-electron scattering.[3-5] When ionized-impurity scattering is dominant in determining mobility, the momentum redistribution among the electrons through electron-electron interactions tends to reduce the mobility.[7-9]

A classical approach to calculating the electron-electron scattering of a completely ionized gas was given by Spitzer and Härm.[10] Starting from the Boltzmann equation with the help of the Fokker-Planck equation, they found that the electron conductivity is reduced by a factor of 0.5816. Another calculation has been made by Appel.[11] Appel used a variational principle with electron-electron scattering a small perturbation. He took the interaction between electrons to be a shielded Coulomb potential. Starting from the Boltzmann equation and calculating up to the second-order terms, Appel found that the electron-electron scattering reduced the Brooks-Herring mobility by a factor of 0.573, independent of temperature.

In this paper, we start from the Kubo formula.[12] As discussed in Fujita,[13] the Kubo formula is reduced to a simpler form which enables us to calculate the ionized-impurity mobility including higher-order scattering effects. Fujita has discussed the general expressions for the conductivity derived from the Kubo formula, including higher-order impurity scattering effects. We use his general expressions to evaluate the effects of high-order impurity scattering in detail, extend his work to derive expressions for the mobility, including electron-electron scattering in all orders, and calculate these effects in detail.

In Sec. II we discuss the Kubo formula briefly and present the results of higher-order impurity